Subgrain boundary structure in melt-textured $R\mathrm{Ba_2Cu_3O_7}$ (R=Y, Nd): Limitation of critical currents versus flux pinning

F. Sandiumenge,[1,*] N. Vilalta,[1] J. Rabier,[2] and X. Obradors[1]

[1]*Institut de Ciència de Materials de Barcelona (CSIC), Campus de la Universitat Autònoma de Barcelona, 08193 Bellaterra, Catalonia, Spain*

[2]*Laboratoire de Métallurgie Physique, UMR 6630, CNRS, Université de Poitiers, SP2MI, Bd 3, Téléport 2, Boîte Postale 30179, F-86962 Chasseneuil Futuroscope Cedex, France*

(Received 20 March 2001; published 19 October 2001)

The microstructure of subgrain boundaries occurring in single-domain $R\mathrm{Ba_2Cu_3O_7}$ (R=Y and Nd) melt-textured composites has been studied by transmission electron microscopy. It is found that subgrain boundaries (SGB's) have a strong tendency to develop parallel to the (100), (010), and {110} planes, while the form of dislocation networks is controlled by the properties of constituting dislocations. In $\mathrm{YBa_2Cu_3O_7}$, presenting one unique glide plane, (001), boundaries stabilized on {110} planes are accommodated by dislocations with lines running along the *c* axis. The occurrence of such an unusual line direction is discussed in terms of the line energy anisotropy on the (001) plane. On the other hand, in $\mathrm{NdBa_2Cu_3O_7}$, with (100), (010), and {110} glide planes in addition to (001), *c*-axis oriented dislocations are also found stabilized on (100)/(010)-faced boundaries. For arbitrary SGB configurations, the form of dislocation networks can be parametrized using the generalized Frank's formula, allowing the calculation of dislocation densities. Besides the underlying dislocation networks, SGB's may develop mesostructures such as faceting and stepped interfaces accommodating the deviation from low-index planes. The way these defects may affect the transport critical currents is discussed on the basis of a simple geometrical model. Since the form of dislocation networks is governed by intrinsic materials parameters, the present results can be extended to other large-scale materials for which a strong incidence of low-angle grain boundary microstructure is anticipated.

DOI: 10.1103/PhysRevB.64.184515 PACS number(s): 74.72.Bk, 74.80.Bj, 61.72.Ff, 61.72.Mm

I. INTRODUCTION

Low-angle grain boundaries appear to have a strong impact on the microstructure and superconducting properties of latest generation large-scale materials, such as melt-textured and coated conductors. In melt-textured $R\mathrm{Ba_2Cu_3O_7}$(R123) composites a dense network of subgrain boundaries (SGB's) prevails even when solidification conditions are optimized such as to obtain a single domain, as demonstrated by the observation of a wide misorientation spread, $\sim 7°$, in directionally solidified bars characterized by a unique and flat growth front.[1–3] Analysis of the rocking curve indicated that this misorientation spread is not only caused by the occurrence of a few discrete SGB's, but contains a strong contribution of a high density of slightly misoriented subgrains.[1] SGB's have misorientations belonging to the very-low-angle regime, mostly in the range $\sim 0.2–5°$, and build up a narrow mosaic substructure. Such a mosaic substructure is then more likely associated with dislocation rearrangements occurring during the cooling process as a result of the plastic anisotropy of the composite[1] and by the interaction of the advancing front with peritectic particles[4] than associated with growth instabilities.[5] Conversely, low-angle GB's in coated conductors appear to be intimately associated with the occurrence of GB's in the underlying substrate,[6] and their generation mechanism is therefore largely controlled by the growth of the layer on a polycrystalline substrate. Despite this difference, however, since the characteristics of GB dislocation networks are governed by the intrinsic structural properties of the material, most of the results presented in this work for melt-textured material are also relevant to GB's in coated conductors.

The mosaic substructure is built by the intersection of SGB's on different planes and the microcracks lying preferentially on (001). Its contribution to the critical currents has not been elucidated yet, but overall it is likely to have a negative effect as suggested by the one order of magnitude gap separating the highest J_c achieved in thin films[7] from the lower values of maximum J_c achieved in single-domain melt-textured Y123.[8] Indeed, electromagnetic studies reveal, as a general trend, that the transport critical current density at zero magnetic field through a GB, J_c^{GB}, is depressed as the misorientation angle θ between grains forming the boundary is increased.[9–18] The simplest model connecting GB microstructure with critical current, the dislocation model, makes the assumption that J_c^{GB} is determined by the area of superconducting channels, or undisturbed material, between dislocation cores.[11,12] Accordingly, above a critical angle $\theta_c = 2\sin^{-1}(|\mathbf{b}|/4r_0)$, r_0 being the radius of the dislocation cores and $|\mathbf{b}|$ the length of the Burgers vector, nonsuperconducting cores overlap and the GB's become a continuous insulating or normal Josephson contact. Conversely, for rotations smaller than θ_c, i.e., in the low-angle regime, experimentally determined $J_c^{\mathrm{GB}}(\theta)$ curves suggest also the distinction between two angular regions, namely a weak dependence up to $3°–7°$ followed by an exponential decline $\propto \exp(-\theta/\theta_0)$ with $\theta_0 = 4°–5°$.[9–18] It appears that the linear dependence $J_c^{\mathrm{GB}}(\theta) = (1-\theta/\theta_c)J_c$ predicted by the dislocation model is only relevant for the very-low-angle regime. In fact, the observed behavior is consistent with models de-

scribing the GB as an array of parallel point contacts[19] that exhibit weak link behavior when their width (or equivalently, the dislocation spacing) becomes smaller than the superconducting coherence length ξ, that is, for $\theta' > |\mathbf{b}|/[\xi(T) - 2r_0]$. That is, for a symmetric tilt boundary on the (100) or (010) planes, $r_0 = |\mathbf{b}| = 3.8$ Å and $\xi_{ab} \sim 35$ Å,[20] one obtains $\theta' \sim 5°$ in agreement with experiment. A realistic analysis of GB properties needs a definition of r_0 with allowance for the precise variation of superconducting properties around the dislocations and therefore should include a detailed picture of the stress distribution and stress-related phenomena such as local T_c and chemical potential changes within the boundary. This issue has been tackled in an elegant model by Gurevich and Pashitski showing that the $J_c^{GB}(\theta)$ dependence is mostly determined by the decrease of the current-carrying cross section by insulating GB dislocation cores and by the progressive local suppression of the superconducting order parameter as the misorientation increases, thus further emphasizing the relevance of the GB dislocation structure on the GB properties.[21] Moreover, regular dislocation networks may appear superimposed by heterogeneous mesostructures typically associated with the development of facets and steps at interfaces. Such mesostructures are typically found in flux-grown[22] and thin-film[23] bicrystals and appear to have relevant implications on the superconducting behavior of the GB's.[24,25] It turns out that any substantial insight into the behavior of the critical currents of melt-textured single domain *R*123, has to connect with a detailed understanding of the defect structure associated with the SGB's. The present study is aimed at contributing to this issue by providing a picture of SGB microstructures on various scale lengths, ranging from the geometry of SGB dislocation networks to mesostructures such as SGB faceting, which introduce sources of heterogeneity on scale lengths ranging from ~10 to ~200 nm. A description of the SGB microstructure in terms of dislocation density is proposed in order to estimate its effect on transport critical current.

II. EXPERIMENT AND RESULTS

Both Y123 [26] and Nd123 [27] melt-textured samples were prepared by directional solidification in air as reported elsewhere. Thin foils were cut from the processed bars, mechanically polished, and ion milled down to electron transparency in a liquid-nitrogen-refrigerated stage in order to minimize damage of the samples. Defect structures where imaged in a transmission electron microscope (TEM) operating at 200 kV using standard diffraction contrast procedures and high-resolution electron microscopy (HREM) imaging.[28] Diffraction contrast images were obtained under identical or similar two-beam conditions in both subgrains forming the SGB in order to get maximum reliability in contrast information from the boundary.[29] Since contrast features described in this paper do not change across the twin boundaries, the notations ⟨100⟩ and {100} will be used for [100], [010] and (100), (010), respectively.

A. Dislocation networks

In the course of the present investigation it has been found that although in Y123 dislocations are most stable on the (001) plane,[30] arrays of *c*-axis-oriented dislocation lines may be stabilized on SGB's. Figure 1(a) presents a $\mathbf{g}=(110)$ dark-field image showing one set of such an array of dislocations stabilized on the {110} plane. [The narrow weak brighter band that crosses the image corresponds to a $(\bar{1}10)$ twin.] In Fig. 1(b) the dislocation lines are seen nearly ends on, revealing intense white/black strain contrasts on the background associated with their strain fields. It can also be observed that the dislocation array bows out when crossing the twin boundary. Since the ⟨110⟩ Burgers vector, derived from contrast analysis, does not change across the {110} twin boundary, the observed bowing of the SGB cannot be explained by dislocation–twin-boundary interactions and other effects such as the occurrence of defects at the twin boundary (e.g., the occurrence of a disordered layer along the twin boundary[31]) should be considered. A detailed explanation of this effect is beyond the scope of the present investigation. By inspection of the [001] selected-area diffraction pattern taken across the boundary plane, a rotation of ~1.5° around the *c* axis was measured. This value is in good agreement with that derived from Frank's formula for a pure tilt boundary using the observed dislocation spacing, $\theta = |\mathbf{b}|/D \sim 1.35°$ (D is the dislocation spacing). On the other hand, as reported previously,[1] SGB's on {100} planes are typically built up by arrays of $\mathbf{b}=\langle 100\rangle$ dislocations with line directions parallel to ⟨010⟩ that can be generated by glide on (001).

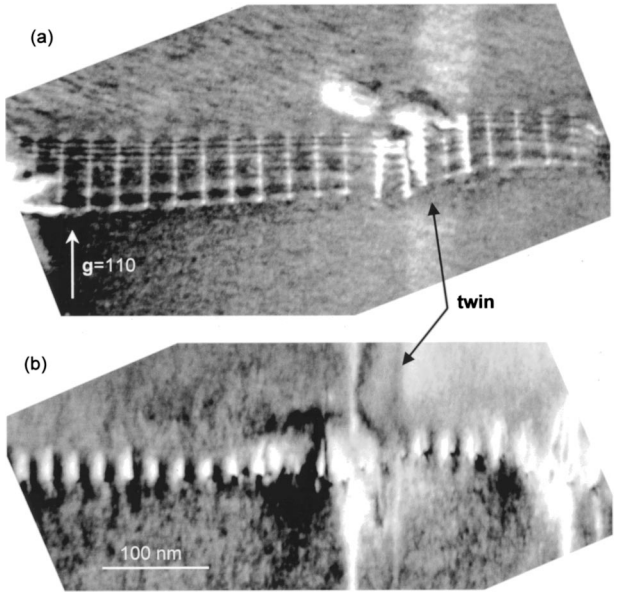

FIG. 1. (a) Dark-field electron micrograph showing a {110} subgrain boundary in Y123 built by an array of $\mathbf{b}=\langle 110\rangle$ dislocations parallel to the *c* axis. (b) Same area as in (a) with dislocations seen nearly end on (electron beam is nearly parallel to [001]).

Figure 2 shows two segments of the same SGB in a Nd123 sample, one aligned with (a) {100} and the other aligned with (b) {110}, accommodated by $\mathbf{b}=\langle 100\rangle$ and $\mathbf{b}\|\langle 110\rangle$ dislocations, respectively. In contrast with the behavior found in Y123, in this case both types of dislocations are aligned with the *c* axis. Different SGB structures are indeed expected owing to the different dislocation behavior

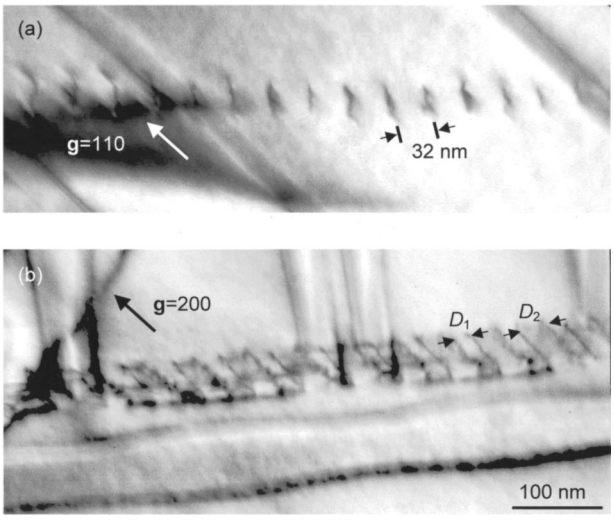

FIG. 2. Bright-field electron micrograph of two segments of the same subgrain boundary in Nd123. (a) Segment built by an array of $\mathbf{b}=\langle 100\rangle$ dislocations parallel to [001] stabilized on the {100} plane. (b) Segment built by an array of $\mathbf{b}\|\langle 110\rangle$ dislocations parallel to [001] stabilized on the {110} plane.

in Nd123 and Y123.[32] The misorientation derived from the dislocation spacing measured in the {100} segment is 0.7°. Careful inspection of Fig. 2(b) reveals two dislocation spacings, $D_1\sim 15$ nm and $D_2\sim 22$ nm. An interpretation of such a bimodal distribution of dislocations considers that $\mathbf{b}=\langle 110\rangle$ dislocations are dissociated into two $\mathbf{b}=\frac{1}{2}\langle 110\rangle$ partial dislocations. Note that a $\mathbf{R}=\frac{1}{2}\langle 110\rangle$ stacking fault formed between the two partial dislocations induces a phase shift on the incident beam $2\pi\mathbf{g}\cdot\mathbf{R}=2\pi$ for $\mathbf{g}=(200)$ and $\mathbf{g}=(110)$ and therefore it will be invisible in diffraction contrast images taken under these conditions. Hence, according to the dissociation hypothesis, the misorientation should be consistent with a dislocation spacing D_1+D_2 between $\mathbf{b}=\langle 110\rangle$ dislocations. This gives 0.8° in agreement with that derived from the dislocation spacing between $\mathbf{b}=\langle 100\rangle$ dislocations in the {100} segment. Dissociated $\mathbf{b}=\langle 110\rangle$ dislocations have been also found in Y123 (see below).

Figure 3 shows diffraction contrast images of a SGB generated by the interaction of two sets of dislocations, $\mathbf{b}_1$ and $\mathbf{b}_2$. When the $\mathbf{g}=(020)$ reflection is excited, one system of almost parallel lines is observed [Fig. 3(a)]. Each line contains two types of dislocation segments with Burgers vectors [010] and [110], and slightly different projected directions. With $\mathbf{g}=(\bar{1}10)$ [Fig. 3(b)], two sets of intersecting dislocations are clearly observed. At the junctions between the two dislocation sets a short segment $\mathbf{b}_3$ is formed leading to a hexagonal network, as shown schematically in Fig. 3(b). The boundary parameters deduced from different projections and $\mathbf{g}\cdot\mathbf{b}$ analysis can be summarized as follows: The misorientation consists of a rotation of ~1.5° around the [001] axis. The boundary-plane normal unit vector in the region shown in the micrographs is $\mathbf{n}=(0.59,0.20,0.78)$. It is useful to express $\mathbf{n}$ in terms of the angles α and β depicted in Fig. 4, as $\mathbf{n}=(\sin\beta\cos\alpha,\sin\beta\sin\alpha,\cos\beta)\equiv(\alpha,\beta)$. In this notation β gives a measure of the twist component. We find n

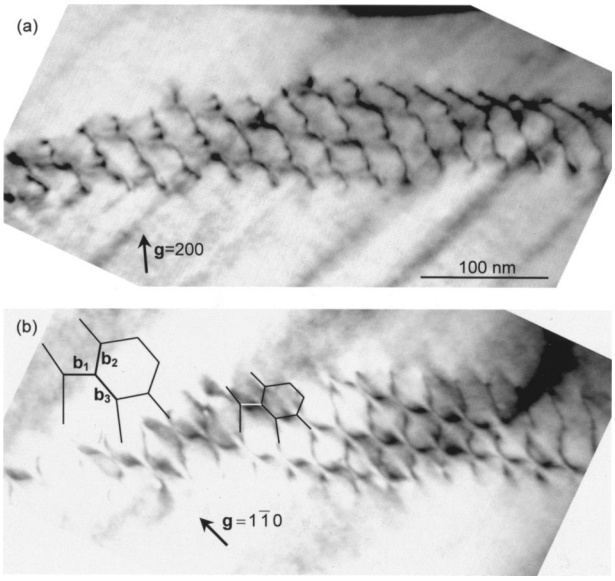

FIG. 3. Bright-field electron micrograph of an hexagonal dislocation network formed by the interaction of $\mathbf{b}_1=[100]$ and $\mathbf{b}_2=[010]$ dislocations. (a) One set of parallel lines. Each line is composed by two dislocation segments with slightly different projections. (b) Three sets of dislocations with coplanar Burgers vectors are visible. The network is stabilized in a plane with arbitrary orientation [$\mathbf{n}=(0.59,0.20,0.78)$] and the rotation axis is [001].

$\equiv(18.64°,38.74°)$. The Burgers vectors of the boundary dislocations are $\mathbf{b}_1=[100]$, $\mathbf{b}_2=[010]$, and $\mathbf{b}_3=\mathbf{b}_1+\mathbf{b}_2=[110]$. We conclude that dislocation $\mathbf{b}_3$ is formed at the junctions between dislocations $\mathbf{b}_1$ and $\mathbf{b}_2$ and that the observed network is a relaxed configuration derived from the interaction of two independent dislocation families, namely, $\mathbf{b}_1$ and $\mathbf{b}_2$.

In the course of the present work we could not find SGB's parallel to the basal plane in TEM specimens cut closely parallel to (001) suitable for diffraction contrast imaging. Instead, Fig. 5 presents a cross-sectional image of a basal plane boundary in Nd123. In Fig. 5(a) the boundary is seen edge on and the lower crystal is ⟨100⟩ oriented, while the upper one, appearing brighter in the image, is slightly misoriented by less than 5°. Note that lattice fringes remain parallel across the boundary, in agreement with a rotation about

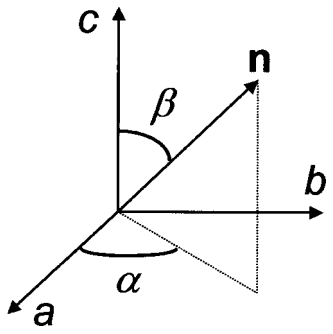

FIG. 4. Representation of the α and β angles relating the orientation of the unit vector perpendicular to the boundary plane, $\mathbf{n}$, with a reference frame linked to the crystallographic axes.

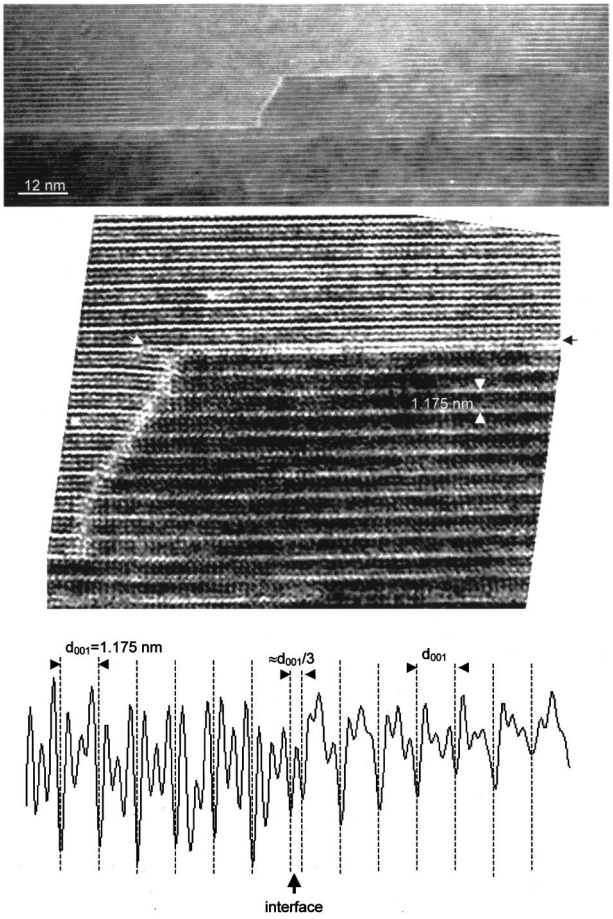

FIG. 5. (a) Basal-faced boundary in Nd123 viewed along ⟨100⟩ showing a step$\sim 10d_{001}$ in height. (b) Magnified view of the region near the step showing a stacking fault with displacement vector $\mathbf{R}=\frac{1}{3}[001]$ at the interface. The extra perovskite layer is indicated by an arrow on the right-hand side of the image. The stacking fault ends slightly away from the step, in the bulk matrix. The associated $\mathbf{b}=\frac{1}{3}[001]$ partial dislocation is indicated by an arrow. (c) Line scan across the interface. Prominent minima correspond to bright fringes in the image. The unit cell is indicated. An extra fringe can be observed at the interface.

the *c* axis. The boundary presents a step ten unit cells in height, across which there is almost prefect continuity between both lattices. Looking at Fig. 5(b) it can be observed that the boundary is associated with a stacking fault consisting of the intercalation of a single perovskite layer (thickness $\frac{1}{3}d_{001}$), as revealed by the occurrence of two consecutive intense bright fringes at the interface. This feature can also be observed in the line scan performed perpendicularly to the boundary, presented in Fig. 5(c). The right-hand side of the scan corresponds to the upper crystal and the minima are located at the bright fringes of the HREM image. The unit cell spacing is indicated by dashed lines, and each unit cell is subdivided into three maxima corresponding to the three perovskite units. The location of an extra fringe disrupting the stacking sequence along the *c* axis across the interface is clearly identified. Careful inspection of the imaged area revealed that the interface stacking fault covers the whole boundary, which accordingly appears to be nonstoichiometric, and ends slightly away from the step, within the bulk matrix. The bounding partial dislocation is indicated by an arrow in the image. Fourier-filtered images of the faulted area indicated that the displacement vector has no component normal to [001] in the plane of the image. Therefore, unless a component normal to the image exists, the stacking fault is characterized by displacement vector $\mathbf{R}=\frac{1}{3}[001]$. It is worth mentioning that similar defects were observed within the bulk matrix, thus suggesting that this is an stable defect not necessarily associated with the interface structure. Similar defects have been previously reported by other authors, suggesting a $BaCuO_2$ composition.[33] The HREM image of Fig. 5 was also used to check the occurrence of lattice strains associated with the boundary. A careful measurement of the spacing between maxima and minima in the line scan of Fig. 5(c) did not reveal strain components normal to the interface, as expected either for a boundary accommodated by a large stacking fault or for a $\theta[001](001)$ twist boundary for which anisotropic elasticity calculations indicate that the normal components of the stress tensor σ_{ii} are zero (with $i=x,y,z$ referred to the crystallographic axes[34]).

B. Subgrain boundary mesostructures

The present investigation has indicated that besides dislocation networks defining the structure on the microscale, nonperiodic mesostructures such as interface steps and boundary facets, introduce sources of heterogeneity on various scale lengths ranging from ~10 to ~200 nm. As an example of faceting, Figs. 6(a)–6(c) show electron micrographs of the same region of a ~0.8° SGB presenting different facets. In all facets dislocations present the same line direction, approximately $[0.06,-0.52,0.27]$. It can be observed that some facet junctions are associated with dark contrasts. An analysis of the nature of these defects is out the scope of the present work, but their occurrence suggests that facet junctions can be associated with significant strains. In Fig. 6(b), taken with $\mathbf{g}=(\overline{1}\,\overline{1}\,0)$ normal to the twins in both subgrains, it can be observed that two dislocations in facet labeled A are out of contrast, thus signaling a Burgers vector parallel to ⟨110⟩. In Fig. 6(c), taken with $\mathbf{g}=(\overline{2}00)$, the same two dislocations are visible and split into two partial dislocations. An enlarged view of the boxed area is shown in the inset, where the two split dislocations are labeled $\mathbf{b}_2$ and the nonsplit dislocation is labeled $\mathbf{b}_1$. The contrast features collected from this region of the SGB indicate that in all facets except facet A the misorientation is accommodated by one array of dislocations with Burgers vector $\mathbf{b}=\langle 100\rangle$, while in facet A the misorientation is accommodated by two parallel arrays of dislocations with Burgers vectors $\mathbf{b}_1=\langle 100\rangle$ and $\mathbf{b}_2\|\langle 110\rangle$. The splitting of $\mathbf{b}_2$ can be attributed to the dissociation of the ⟨110⟩ Burgers vector into two partial dislocations with Burgers vectors $\frac{1}{2}\langle 110\rangle$, as also reported for a flux grown bicrystal[22] and a thin-film GB.[35]

Deviations from the orientation of low-index planes, {100} and {110}, is frequently found to be accommodated by interface steps. Figures 7(a) and 7(b) are bright-field electron micrographs of a stepped ~5.5°⟨100⟩ SGB with ledges parallel to {100}. In both images the lower subgrain, **g**

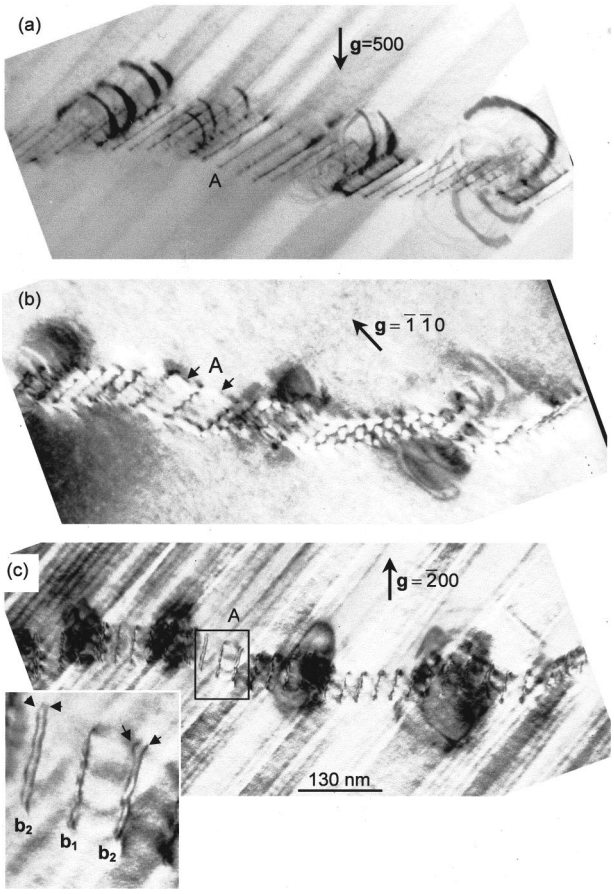

FIG. 6. Bright-field electron micrographs of a faceted subgrain boundary in Y123. (a) $\mathbf{g}=(500)$. (b) $\mathbf{g}=(\bar{1}\,\bar{1}\,0)$. (c) $\mathbf{g}=(\bar{2}00)$. The inset shows a detail of the split $\mathbf{b}=\frac{1}{2}\langle 110\rangle$ dislocations appearing in facet labeled *A*.

$=(110)$, is normal to the twins, while the upper subgrain is under a multibeam condition. Figure 7(b) shows how the size of the steps varies with the macroscopic orientation of the boundary. The black/white contrast fringes parallel to the boundary plane arise from the superposition of a strongly diffracting subgrain with a weakly diffracting subgrain[36] and are not related to the defect structure. Careful inspection reveals significant strain contrast at the microfacet junctions, as also reported for flux-grown bicrystals.[22] The presence of boundary steps otherwise indicates a possible mechanism of SGB migration.

III. DISCUSSION

A. SGB dislocation networks in *R*123

Our observations indicate that SGB's formed by one set of dislocations present a strong tendency to develop on planes of the type {100} and {110}. Indeed, anisotropic elasticity calculations[30] for Y123 show that stable dislocations lie on the (001) plane and present ⟨100⟩ and ⟨110⟩ Burgers vectors. However, dislocations with $\mathbf{b}=\langle 110\rangle$ are stable in the screw orientation.[30] As a result of this anisotropic character of the dislocations, the mechanism involved in the formation of SGB's on {100} planes differs from that corresponding to

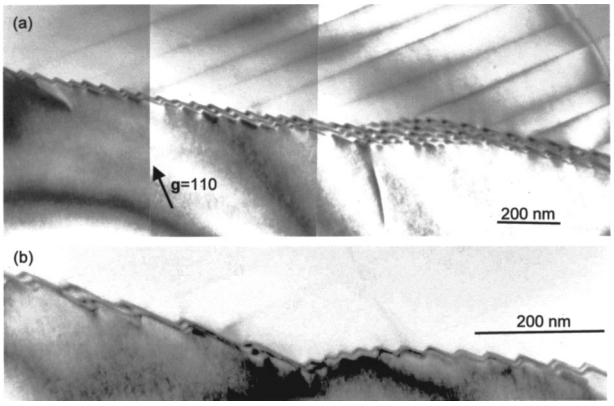

FIG. 7. Bright-field electron micrographs of a stepped subgrain boundary in Y123. The upper grain is a multibeam condition while the lower grain is imaged with $\mathbf{g}=(110)$ normal to the twins. Steps are parallel to {100} planes and accommodate the deviation of the macroscopic orientation of the boundary from the low-index plane. Strain contrast at the step is visible. In (b) it can be clearly observed that the size of the steps is decreased as the deviation of the macroscopic SGB plane from {100} increases.

{110}-type SGB's. Indeed, arrays of edge dislocations with [100] and [010] Burgers vectors can be stabilized on (100) and (010) planes by a simple glide operation on (001), although in general the climb has to occur at sufficiently high temperatures in order to achieve a low-energy configuration. The resulting configuration provides a net Burgers vector normal to the dislocation wall necessary to accommodate the misorientation across the SGB. The situation with $\mathbf{b}=\langle 110\rangle$ dislocations is different because they find an energy minimum in the screw orientation. Accordingly, a stack of $\mathbf{b}=\langle 110\rangle$ dislocations on {110} (with dislocation lines parallel to **b**) would not provide a Burgers vector normal to the dislocation wall and therefore cannot be stabilized on a SGB unless their dislocation lines climb out of the (001) plane.[37] Indeed, such dislocations lines, when arranged in SGB's, have always been found lying parallel to [001] and arranged on the {110} plane. Note that the generation of such boundaries involve, together with a climb component, the activation of secondary glide systems like $\langle 110\rangle(1\bar{1}0)$. In Nd123, the occurrence of {100} and {110} glide planes in addition to (001) suppresses the distinction noted above between the generation mechanisms of SGB's on {100} and {110} planes.

According to the dislocation model, the relevant parameter determining the critical current transported across a GB is its dislocation density, $\rho=1/D$ (D is the dislocation spacing), which for a pure symmetrical tilt GB is $\sim\theta/|\mathbf{b}|$. For an arbitrary GB, the general form of Frank's formula allows the prediction of the geometry of possible precursor dislocation arrays. The following relation holds for a general boundary:[38]

$$\mathbf{d}=2\sin\left(\frac{\theta}{2}\right)(\mathbf{p}\otimes\mathbf{r})\approx\theta(\mathbf{p}\otimes\mathbf{r}), \tag{1}$$

where **p** is an arbitrary vector contained in the plane of the boundary, **d** is the sum of the Burgers vectors intersected by **p**, and **r** is a unit vector along the rotation axis. For two sets

of dislocations $\mathbf{d}=n_1\mathbf{b}_1+n_2\mathbf{b}_2$, where n_1 and n_2 are the number of dislocations of each type intersected by **p**. From Eq. (1) it follows that **r** is perpendicular to the plane defined by $\mathbf{b}_1$ and $\mathbf{b}_2$,[38] as is the case of the example shown in Fig. 3. This consideration predicts that in *R*123, where the most stable Burgers vectors lie on the (001) plane, SGB's generated by two sets of intersecting dislocations will present a strong tendency to rotate about [001], while there is no constraint on the boundary plane orientation.

Consider the SGB shown in Fig. 3, built by $\mathbf{b}_1=[100]$ and $\mathbf{b}_2=[010]$ dislocations, and neglect their interaction. The dislocation line directions $\mathbf{l}_1$ and $\mathbf{l}_2$ are given by $\mathbf{b}_2\times\mathbf{n}$ and $\mathbf{b}_1\times\mathbf{n}$, respectively. In the present case they can be expressed in terms of α and β, $\mathbf{l}_1=(\cos\beta,0,\sin\beta\cos\alpha)$ and $\mathbf{l}_2=(0,-\cos\beta,\sin\beta\sin\alpha)$, i.e., the dislocations form a square network for $\alpha=0°,90°$ and all values of β, except for $\beta=90°$ when one of the dislocation sets (that with the Burgers vector contained in the boundary plane) disappears and the geometry transforms to that of a symmetrical tilt boundary. For all other orientations of **n** the dislocation array forms an oblique network as in the present case. Applying the formulas given in Ref. 38, the orientation-dependent dislocation density, $\rho_T(\mathbf{n})=\rho_1(\mathbf{n})+\rho_2(\mathbf{n})$, can be expressed as

$$\rho_T(\mathbf{n})=\frac{\theta}{a}(A+B), \tag{2}$$

where for simplicity we take a tetragonal lattice, i.e., $a=b$. The first factor represents the dislocation density of a pure tilt boundary and the second one is a geometrical factor that takes into account the deviation from the tilt geometry given by $A=\sqrt{\cos^2\beta+\sin^2\beta\cos^2\alpha}$ and $B=\sqrt{\cos^2\beta+\sin^2\beta\sin^2\alpha}$. This gives $\rho_T=1.78\theta/a$ for the above example, i.e., the dislocation density is increased by a factor $\approx$1.8 relative to a SGB having the same rotation angle but a symmetrical tilt geometry. This value is of course slightly affected by the interaction leading to segments of dislocation 3. It is interesting to note that if only dislocation glide is allowed, two sets of dislocations can only build an arbitrary SGB if there are two active glide planes, as would be expected for Nd123.[32] A complete arbitrary boundary (that is, with arbitrary orientation of the rotation axis and boundary plane normal) can be generated by means of three sets of linearly independent Burgers vectors. In Y123 compounds, the most stable Burgers vectors lie on the basal plane[30] and therefore the formation of complete arbitrary boundaries is not probable. Such a boundary should be constructed on a basis having Burgers vectors $\mathbf{b}_1=a[100]$, $\mathbf{b}_2=b[010]$, $\mathbf{b}_3=(c/3)[001]$, which correspond to the edges of the (pseudo-) cubic perovskite unit. The $(c/3)[001]$ Burgers vector in fact results from the dissociation into three collinear partials of a perfect dislocation with $c[001]$ Burgers vector, which owing to the length of c has a prohibitive strain energy. To the authors' knowledge, there is only one example of one low-angle GB constituted by a combination of these Burgers vectors, leading to five sets of dislocations.[39]

On the (001) plane, the most likely SGB that can be formed is a twist boundary consisting of a square grid of $\mathbf{b}=\langle 110\rangle$ screw dislocations, while the formation a tilt boundary would involve the climb dissociation of $\mathbf{b}=[001]$ dislocations into three collinear $\frac{1}{3}[001]$ partial dislocations as observed in polycrystalline samples.[40] However, to the authors' knowledge there are no reports on such dislocation networks stabilized on basal boundaries in melt-textured materials. This is likely due to the preferential development of microcracks on (001). On the other hand, the unique basal boundary found in the course of the present investigation (Fig. 5), containing a large stacking fault with displacement vector $\mathbf{R}=\frac{1}{3}\langle 001\rangle$, is more likely associated with a growth defect.

B. Subgrain boundary mesostructures

In the preceding paragraphs we have considered the SGB's as regular dislocation networks. However, a complete picture of the SGB microstructure must also include the morphological features of the SGB, characterized by stepped interfaces (Fig. 7) and faceting (Fig. 6), that constitute sources of microstructural heterogeneity in various length scales. Similar sources of microstructural heterogeneity have been reported for flux-grown[22] and thin-film[23] low-angle Y123 bicrystals.

Stepped interfaces also occur in melt-textured materials in order to accommodate deviations of the macroscopic plane from the low-index orientation (Fig. 7). Steps and ledges are comprised of flat low-index facets with lengths in the range 10–150 nm, depending on the local orientation of the macroscopic plane, as clearly shown in Fig. 7(b). The occurrence of steps may be an indication of the migration of the SGB at high temperatures under the action of thermal and/or stress gradients, most likely during the initial cooling stages from the solidification temperature, and are therefore likely to represent kinetically frozen-in configurations. In this sense, some aspects of their microstructure resemble those reported for flux-grown bicrystal boundaries exhibiting sawtooth structures[22] or even those commonly observed thin-film bicrystal boundaries, which are typically found to meander along the path of the underlying straight substrate boundary,[33] each meander being comprised by similar facets as well. Nevertheless, stepped interfaces in melt-textured *R*123 are, in general, more regular than thin-film meandering boundaries as otherwise expected owing to the fact that thin-film GB's form under growth conditions far from equilibrium.

Since the orientation of the plane of a SGB determines the nature of dislocations stabilized on it, different facets in a faceted SGB may contain different types of dislocations. Facets may arise from the local incorporation of another type of dislocation into the SGB. These parts of SGB's rotate in order to minimize the dislocation energies. As an example, Fig. 6 shows that facet A includes $\mathbf{b}=\langle 110\rangle$ dislocations, in addition to $\mathbf{b}=\langle 100\rangle$ ones, that appear split into $\frac{1}{2}\langle 110\rangle$ partial dislocations. Notably, we have found that not all the observed $\mathbf{b}=\langle 110\rangle$ SGB dislocations are split (e.g., Fig. 1). This distinctive behavior is likely to be related to the fact that the splitting of $\mathbf{b}=\langle 110\rangle$ SGB dislocations results from a climb dissociation requiring high temperatures and therefore depends on the temperature of formation of the boundary. On

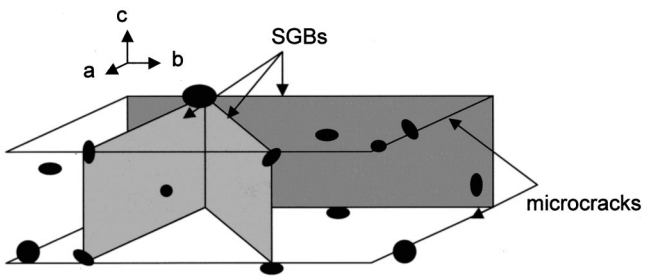

FIG. 8. Idealized drawing of the mosaic substructure of melt-textured *R*123 materials, defined by the intersection of SGB's (shadowed) and microcracks. Black particles are peritectic inclusions.

the other hand, the width of the stacking-fault ribbon is determined by a balance between the repulsive force between the partial dislocations and the stacking-fault energy depending on the particular facet where the dissociation takes place. Looking at the crystal structure of Y123 one finds that a slab of thickness $\frac{1}{2}d_{110}$ is composed by a stack of planes of the type *A*-*B*-*A*-*B*, where *A* has a composition $YBa_2Cu_3O_2$ and *B* is O_5. Therefore, a $\mathbf{R}=\frac{1}{2}\langle 110\rangle$ stacking fault has a stoichiometric composition on the (110) plane. However, the same **R** results in a violation of the Cu-Ba first-neighbor order and a high stacking-fault energy is expected. On the other hand, for dissociation planes other than {110}, deviations from stoichiometry are likely to be associated with an increase of the stacking-fault energy in agreement with the narrow splitting width observed in Fig. 6(c). In a GB, the splitting width may also vary with position in a particular facet due to an inhomogeneous stress distribution within facets of small dimensions[22] and with θ.[41]

C. Implication of observed SGB dislocation networks on critical currents

According to our observations, a three-dimensional picture of the mosaic structure may be drawn as defined by the intersection of dislocation walls, displaying a tendency to align with {100} and {110} planes, with microcracks lying parallel to (001) (Fig. 8). Polarized light observations[42,43] indicate that the size of the subgrains is tuned by the size and concentration of peritectic particles.[44] TEM images indicate that in sample regions having a high density of particles, subgrains can be as small as a few micrometers.[1] Thus the current flowing on the (001) plane must always cross SGB's, while the current flowing parallel to the *c* axis will be mainly limited by microcracks. In Nd123, however, {100} and {110} microcracks also develop, though to a lesser extent than (001) microcracks.[45] The effect of the SGB's on the critical current is controlled by their microstructure, which typically consists of more or less heterogeneous mesostructures superposed on an ideally regular dislocation network.

For symmetrical tilt GB's, the dislocation model states that in the low-angle regime ($\theta<\theta_c$) the transport current across the GB is proportional to the area of superconducting undisturbed material between dislocations. Taking into account the elastic strain fields, an effective radius of the non-superconducting core of the GB dislocations, $r_{\rm eff}$, can be

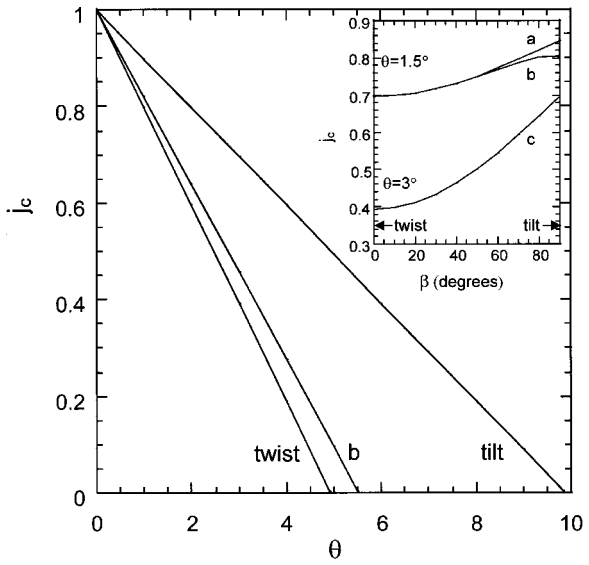

FIG. 9. Plot of Eq. (2) for different boundary plane orientations. Curve *b* refers to $\mathbf{n}=(0.59,0.20,0.78)$ as determined for the subgrain boundary shown in Fig. 3. The inset shows the effect of adding a twist component to an initial tilt configuration on the (100) plane with misorientations of 1.5° (curve *a*) and 3° (curve *c*). Curve *b* is computed for $\alpha=18.64°$ (see text).

defined such that the observed behavior can be approximately described by $j_c(\theta)=1-2r_{\rm eff}\theta/|\mathbf{b}|$,[12] where j_c is the ratio of the grain boundary to intragrain critical current. The best fit with experimental data is obtained for $r_{\rm eff}=2.9|\mathbf{b}|$.[12] In order to extend the model to GB's with arbitrary geometry it is interesting to note that the factor $\theta/|\mathbf{b}|$ in fact describes the dislocation density ρ (or inverse of the dislocation spacing) in the GB. Thus, we can write $j_c(\rho)=1-2r_{\rm eff}\rho_T$. From this relation it can be expected that two boundaries having the same rotation but different dislocation densities (i.e., a different geometrical relationship between the rotation axis and the boundary plane normal) will present different values of their critical current. Taking, for instance, a boundary with rotation axis [001] composed of two sets of dislocations with Burgers vectors $a[100]$ and $a[010]$ ($a\sim b$) and the boundary plane normal given by $\mathbf{n}=(\alpha,\beta)$ as in the example considered above, using Eq. (2) we find

$$j_c(\mathbf{n})=1-2r_{\rm eff}\,\frac{\theta}{a}(A+B), \tag{3}$$

where *A* and *B* are geometrical factors that take into account the orientation of the boundary plane normal, as defined in the preceding section. For $\beta=90°$ and $\alpha=0°$, 90° the arbitrary boundary transforms to a symmetric tilt boundary. According to Eq. (2), the introduction of a twist component, i.e., for $\beta<90°$, has a strong effect on the width of superconducting undisturbed channels between dislocations. This is shown in Fig. 9 where j_c [Eq. (3)] is plotted for the pure tilt configuration on (100), the SGB plane determined for the example shown in Fig. 3 (indicated by *b*), and the twist configuration on (001). Note that the misorientation needed to achieve a given j_c ratio is nearly halved for the twist or the

present example (Fig. 3) configurations. The effect of the twist component is enhanced by the magnitude of the misorientation. The inset clearly shows this feature for $\theta=1.5°$ and $\theta=3°$, as well as the fact that the decay in j_c is stronger for $\beta>45°$ and is smoothed out as the boundary approaches the twist configuration. Accordingly, the suppression of superconducting cross-sectional area for a boundary having ~57% twist character (curve *b*) is similar to that expected for the pure twist configuration. In the inset *a* and *c* refer to an initially pure tilt on the (100) plane rotated about [100] by β up to the twist configuration, and curve *b* is computed for $\alpha=18.64°$ as for the example presented in Fig. 3. Thus, in a $\theta=3°$ boundary with 50% twist character ($\beta=45°$) approximately 50% of its cross-sectional area is disturbed by boundary dislocations, while in a tilt SGB the same rotation implies only a 30% reduction of superconducting cross-sectional area and therefore in j_c. As the boundary plane approaches (001), however, the situation is complicated by the elastic anisotropy[46] of Y123 and the layered structure of the compound, which together may favor the localization of the mismatch strain on a length scale similar to the thickness of the insulating slab of the unit cell. An extreme case of this situation is found in the highly anisotropic compound Bi/2212, where this effect has been proposed to explain the observed misorientation-independent superconducting behavior of (001) twist boundaries.[34] Following similar arguments, the effect of nonstoichiometry in a basal plane SGB (Fig. 5) on J_c^{GB} is expected to be weak because the thickness of the inserted layer, $\mathbf{R}=\frac{1}{3}(001)$, ~0.39 nm, is similar to the superconducting coherence length along the *c* axis, $\xi_c=0.3$ nm,[20] and because its effect is also likely to be masked by the intrinsic anisotropy. On the other hand, (001)-faced boundaries occurring in melt-textured *R*123 are likely to have only a weak incidence on the bulk superconducting behavior because their effect is masked by the extended (001) microcracking.

In the discussion of the preceding paragraph, it has been assumed that the dislocation model is valid through the whole low-angle regime. However, experimentally determined $J_c^{GB}(\theta)$ curves for tilt GB's suggest an exponential decay for misorientations greater than $\theta'=3°-7°$,[9–17] which has been modeled by describing the boundary as an array of point contacts exhibiting weak link behavior when their width becomes smaller than ξ.[19] Translating this model to an array of straight parallel dislocations one obtains $\theta'=|\mathbf{b}|/[\xi(T)-2r_0]\sim 5°$ in agreement with experiment. Since the misorientations found in SGB's typically fall below θ', those SGB's displaying a symmetrical tilt configuration are likely to induce only a weak depression of the transport critical current across the SGB. Conversely, deviations from the symmetrical tilt geometry are likely to shift the θ' value to lower misorientations, towards the angular range where a more significant contribution from SGB dislocation networks is expected. Unfortunately, a redefinition of θ' for arbitrary SGB configurations is not straightforward. A tentative estimation is, however, easy to perform in terms of dislocation densities. Consider again the SGB plane normal derived for the SGB shown in Fig. 3. In this case one finds that θ' is shifted down to ~2.8°, i.e., closer to typical SGB misorientations. Obviously this simple geometrical approach does not take into account the dislocation interactions as those observed in Fig. 3 or the stress distribution within the SGB plane generated by two sets of intersecting dislocations, which otherwise would tend to further reduce the current-carrying cross-sectional area of the SGB. This approach therefore predicts that some SGB's may cause an exponential decay of transport critical current even in the very-low-angle regime and hence have a stronger influence on the critical current than that expected for the linear regime represented in Fig. 9.

As found in the present study, SGB dislocations may be dissociated [Figs. 2(b) and 6]. As far as the superconducting properties of the SGB's are concerned, dislocation splitting has two remarkable effects, namely the dislocation density is increased and a stacking-fault ribbon is created between the two partial dislocations. As argued by Tsu, Babcock, and Kaiser,[22] one can assume that the stacking-fault ribbons do not affect the superconducting coupling across the boundary due to their localization in the direction of the current. On the other hand, taking $r_0=|\mathbf{b}|$ and noting that $|\mathbf{b}|$ is halved upon dissociation, it is found that the superconducting cross-sectional area of the boundary is not changed. Then, the only effect of dislocation splitting on the superconducting properties of the SGB is associated with the decrease of the dislocation spacing, which for a given SGB plane orientation and misorientation, may cause a downward shift of θ' in a way similar to that discussed above in connection with variations of **n** at constant misorientation.

The contribution of SGB dislocation networks to the field dependence of the critical currents in melt-textured materials is complex to analyze and it should be discussed in connection with the geometry and the physical characteristics of the measurement technique. For instance, defects such as those shown in Figs. 1 and 2 provide evenly spaced arrays of dislocations parallel to the *c* axis that are likely to act as strong pinning centers for flux lines oriented parallel or perpendicular to them if the Lorentz force has a component perpendicular to the SGB plane. Note that in Y123, where the dislocation glide is confined onto a unique glide plane, namely (001), {110} SGB's (Fig. 1) are the unique natural structures that could provide *c*-axis correlated disorder pinning.[47] The situation is different in Nd123 where the occurrence of {100} and {110} additional glide planes favors the stabilization of *c*-axis dislocations in SGB's parallel to those planes (e.g., Fig. 2) that are expected to enhance the pinning strength when the magnetic field is parallel to the *c* axis. The pinning efficiency of similar configurations has been assessed using a symmetrical tilt 4° bicrystal Y123 film.[48] On the other hand, the same dislocation array can be considered as a limiting mechanism for transport J_c flowing on the (001) plane or for the low-field inductive critical current $J_c^{ab}(0,T)$, as discussed above.

Besides regular dislocation networks, mesoscale structures such as faceting or stepped interfaces associated with curved interfaces may have important implications on the superconducting properties of the boundary. The effect of such mesostructures on J_c^{GB} is independent of, but may be

superimposed on, the contribution of SGB dislocation networks. An extreme situation is found in thin-film bicrystals characterized by meandering interfaces. Such boundaries present a GB critical current enhancement by a factor of 30 relative to flat bulk biseeded GB's for θ values up to 30°,[24] which has been attributed to the differences of the pinning of Josephson vortices in meandering and flat GB's.[24] A further interesting phenomenon associated with interfacial mesostructures was reported for a flux-grown Y123 bicrystal displaying a sawtoothed faceted structure. Long-range strains originating at facet junctions, similar to those observed in Fig. 7, may cause a modulation of $T_c(\mathbf{r})$ along the path of the boundary. In this way, faceting can modulate the coupling strength of GB's and the strains concentrated around facet junctions can substantially increase the critical current at high fields by a field-induced pinning mechanism.[25] On the other hand, *d*-wave symmetry effects[49] of the order parameter that contribute to depress J_c^{GB} induce only a weak misorientation dependence $\propto \cos^2 2\theta$ of the critical current and are therefore likely to induce a minor effect compared to that associated with the SGB dislocation networks in the low-angle regime.

Our microstructural observations clearly show that SGB's within single melt-textured domains are not necessarily as flat as those obtained by a biseeding technique,[50] but present mesostructures that according to detailed GB studies in other materials may lead to substantial enhancements of their superconducting behavior compared to those expected from a description in terms of dislocation content and misorientation only as that given in the preceding section. Unfortunately, we cannot provide in this work a statistical picture of the distribution of the different types of SGB microstructures and mesostructures, but the present results strongly suggest that the field dependence of the SGB critical current is governed by the competition of the different types of defects.

IV. CONCLUSIONS

TEM observations of the microstructure of SGB's in melt-textured Y123 and Nd123 materials reveal that SGB dislocation arrays are restricted to a few configurations on the {100} and {110} planes. Therefore, critical currents flowing on (001) must always cross SGB's. Such configurations can be directly inferred from the highly anisotropic crystal structure of 1-2-3-like superconductors, namely, preferred SGB planes are those perpendicular to the most stable Burgers vectors $\mathbf{b}=\langle 100\rangle$ and $\mathbf{b}=\langle 110\rangle$ and therefore to the prominent glide plane, (001). In Y123, with (001) as unique prominent glide plane, SGB's on {110} are built by *c*-axis oriented $\mathbf{b}=\langle 110\rangle$ dislocations. The formation of {110} SGB's is therefore likely to be more restrictive as it involves, in addition to a climb component, the activation of a secondary glide system, $\langle 110\rangle$ {110}. The occurrence of the unusual *c*-axis orientation can be explained taking into account the line energy anisotropy of $\mathbf{b}=\langle 110\rangle$ dislocations on the (001) plane. In Nd123, with {100} and {110} glide planes in addition to (001), *c*-axis oriented dislocations are found either on {100} or {110} SGB's. Incorporation of additional dislocations may stabilize the SGB on planes with arbitrary orientation. Regular dislocation arrays are frequently superposed by SGB mesostructures, typically facets and steps, that break the periodicity of the dislocation array on length scales ranging from $\sim$10 to $\sim$200 nm.

Dislocation contents in arbitrary SGB's built by two sets of dislocations can be estimated using the generalized Frank formula. Extrapolation of the j_c dependence on dislocation density (or misorientation) experimentally determined for symmetric tilt GB's to arbitrary SGB's, predicts a significant depression of critical current as the twist component of the boundary is increased at constant misorientation. Conversely, in light of experimental studies, the occurrence of mesostructures is likely to enhance the critical current in high fields. The topology of the mosaic substructure along with the observed SGB microstructure strongly suggests that SGB networks in melt-textured materials may limit significantly the critical current at zero field, while at higher fields its contribution is likely to result from the interplay between the underlying dislocation array and mesostructures.

ACKNOWLEDGMENTS

This work has been supported by Supercurrents (EU, TMR Network ERBFMRXCT98, 0189), CICYT (MAT99, 0855), and Generalitat de Catalunya, CNRS (PIC).

*Corresponding author. Electronic address: F. S. felip@icmab.es

[1] F. Sandiumenge, N. Vilalta, X. Obradors, S. Piñol, J. Bassas, and Y. Maniette, J. Appl. Phys. **79**, 8847 (1996).

[2] F. Sandiumenge, B. Martínez, and X. Obradors, Supercond. Sci. Technol. **10** (10th anniversary of high T_c superconductivity special issue), A219 (1997).

[3] P. Diko, N. Pellerin, and P. Odier, Physica C **247**, 169 (1995).

[4] P. Diko, S. Takebayashi, and M. Murakami, Physica C **297**, 216 (1998).

[5] E. Sudhakar Reddy and T. Rajasekharan, Phys. Rev. B **55**, 14 160 (1997).

[6] D. M. Feldman, J. L. Reeves, A. A. Polyanskii, G. Kozlowski, R. R. Biggers, R. M. Nekkanti, I. Maartense, M. Tomsic, P. Barnes, C. E. Oberly, T. L. Peterson, S. E. Babcock, and D. C. Larbalestier, Appl. Phys. Lett. **77**, 2906 (2000).

[7] B. Dam, J. M. Huijbregtse, F. C. Klaassen, R. C. F. van der Geest, G. Doornbos, J. H. Rector, A. M. Testa, S. Freisem, J. C. Martínez, B. Stäuble-Pümpin, and R. Griessen, Nature (London) **399**, 439 (1999).

[8] P. X. Zhang, H. W. Weber, and L. Zhou, Supercond. Sci. Technol. **8**, 701 (1995); E. Mendoza, T. Puig, E. Varesi, A. E. Carrillo, J. Plain, and X. Obradors, Physica C **334**, 7 (2000); T. Puig, J. Plain, F. Sandiumenge, X. Obradors, J. A. Alonso, and J. Rabier, Appl. Phys. Lett. **75**, 1952 (1999).

[9] For reviews focusing on grain-boundary microstructure-property correlations see S. E. Babcock and J. L. Vargas, Annu. Rev. Mater. Sci. **25**, 193 (1995); S. E. Babcock, Micron **30**, 449 (1999).

[10] M. B. Field, D. C. Larbalestier, A. Parikh, and K. Salama, Physica C **280**, 221 (1997).

[11] D. Dimos, P. Chaudhari, J. Mannhart, and F. K. LeGoues, Phys. Rev. Lett. **61**, 219 (1988); Phys. Rev. B **41**, 4038 (1990).
[12] M. F. Chisholm and S. J. Pennycook, Nature (London) **351**, 47 (1991).
[13] Z. G. Ivanov, P. A. Nilsson, D. Winkler, J. A. Alarco, T. Claeson, E. A. Stepantsov, and A. Ya. Tzalenchuk, Appl. Phys. Lett. **59**, 3030 (1991).
[14] R. Gross, in *Interfaces in High-T_c Superconducting Systems*, edited by S. L. Shinde and D. A. Rudman (Springer, New York, 1994), p. 176.
[15] D. T. Verebelyi, D. K. Christen, R. Feenstra, C. Cantoni, A. Goyal, D. F. Lee, M. Paranthaman, P. N. Arendt, R. F. DePaula, J. R. Groves, and C. Prouteau, Appl. Phys. Lett. **76**, 1755 (2000).
[16] N. F. Heinig, R. D. Redwing, J. E. Nordman, and D. C. Larbalestier, Phys. Rev. B **60**, 1409 (1999).
[17] T. Amerin, L. Schultz, B. Kabius, and K. Urban, Phys. Rev. B **51**, 6792 (1995).
[18] D. T. Verebelyi, C. Cantoni, J. D. Budai, D. K. Christen, H. J. Kim, and J. R. Thompson, Appl. Phys. Lett. **78**, 2031 (2001).
[19] E. Sarnelli, P. Chaudhari, and J. Lacey, Appl. Phys. Lett. **62**, 777 (1992); B. H. Moeckly, D. K. Lathrop, and R. A. Buhrman, Phys. Rev. B **47**, 400 (1993); E. A. Early, R. L. Steiner, A. F. Clark, and K. Char, *ibid.* **50**, 9409 (1994).
[20] U. Welp, W. K. Kwok, G. W. Crabtree, K. G. Vandervoort, and J. Z. Liu, Phys. Rev. Lett. **62**, 1908 (1989).
[21] A. Gurevich and E. A. Pashitskii, Phys. Rev. B **57**, 13 878 (1998).
[22] I-Fei Tsu, S. E. Babcock, and D. L. Kaiser, J. Mater. Res. **11**, 1383 (1996).
[23] D. J. Miller, T. A. Roberts, J. H. Kang, J. Talvacchio, D. B. Buchholz, and R. P. H. Chang, Appl. Phys. Lett. **66**, 2561 (1995).
[24] K. E. Gray, M. B. Field, and D. J. Miller, Phys. Rev. B **58**, 9543 (1998).
[25] X. Y. Cai, A. Gurevich, I. Fei Tsu, D. L. Kaiser, S. E. Babcock, and D. C. Larbalestier, Phys. Rev. B **57**, 10 951 (1998).
[26] S. Piñol, F. Sandiumenge, B. Martínez, V. Gomis, J. Fontcuberta, X. Obradors, E. Snoeck, and Ch. Roucau, Appl. Phys. Lett. **65**, 1448 (1994).
[27] R. Yu, F. Sandiumenge, B. Martínez, N. Vilalta, and X. Obradors, Appl. Phys. Lett. **71**, 413 (1997).
[28] D. B. Williams and C. B. Carter, *Transmission Electron Microscopy* (Plenum, New York, 1996).
[29] P. Humble and C. T. Forwood, Philos. Mag. **31**, 1011 (1975).
[30] J. Rabier, in *Plastic Deformation of Ceramics*, edited by R. C. Bradt, C. A. Brooks, and J. L. Routbort (Plenum, New York, 1995), p. 403.
[31] Y. Zhu, M. Suenaga, and Y. Xu, Philos. Mag. Lett. **60**, 51 (1989).
[32] F. Sandiumenge, N. Vilalta, J. Rabier, and X. Obradors, Appl. Phys. Lett. **73**, 2660 (1998).
[33] H. Wu, M. J. Kramer, K. W. Dennis, and R. W. McCallum, Appl. Phys. Lett. **71**, 3572 (1997).
[34] Y. Zhu, Q. Li, Y. N. Tsay, M. Suenaga, G. D. Gu, and N. Koshizuka, Phys. Rev. B **57**, 8601 (1998).
[35] Y. Gao, K. L. Merkle, G. Bai, H. L. M. Chang, and D. J. Lam, Ultramicroscopy **37**, 326 (1991).
[36] R. C. Pond, J. Microsc. **135**, 213 (1984).
[37] See, e.g., J. B. Hirth and J. Lothe, *Theory of Dislocations* (McGraw-Hill, New York, 1968).
[38] S. Amelinckx and W. Dekeyser, Solid State Phys. **8**, 325 (1959).
[39] Y. Zhu, Philos. Mag. A **69**, 717 (1994).
[40] M. F. Chisholm and D. A. Smith, Philos. Mag. A **59**, 181 (1989).
[41] H. Kung, J. P. Hirth, S. R. Foltyn, P. N. Arendt, Q. X. Jia, and P. Maley, Philos. Mag. Lett. **81**, 85 (2001).
[42] F. Sandiumenge, S. Piñol, X. Obradors, E. Snoeck, and Ch. Roucau, Phys. Rev. B **50**, 7032 (1994).
[43] P. Diko, W. Gawalek, T. Habisreuther, Th. Klupsch, and P. Görnert, Phys. Rev. B **52**, 13 658 (1995).
[44] Indeed, a narrowing of the subgrain size on the (001) plane is expected because the addition of peritectic particles increases the density of perfect dislocations nucleated at their interfaces, while their size along the *c* axis is also decreased because peritectic particles also promote the nucleation of microcracks as proposed by P. Diko, Supercond. Sci. Technol. **11**, 68 (1998).
[45] N. Vilalta, F. Sandiumenge, R. Yu, and X. Obradors, in *Applied Superconductivity 1997*, Inst. Phys. Conf. Series No. 158, edited by H. Rogalla and D. H. A. Blank (Institute of Physics, London, 1997), p. 853
[46] H. Ledbetter and M. Lei, J. Mater. Res. **6**, 2253 (1991).
[47] D. R. Nelson and V. M. Vinokur, Phys. Rev. B **48**, 13 060 (1993).
[48] A. Díaz, L. Mechin, P. Berghuis, and J. E. Evetts, Phys. Rev. Lett. **80**, 3855 (1998).
[49] H. Hilgenkamp, J. Mannhart, and B. Mayer, Phys. Rev. B **53**, 14 586 (1996).
[50] V. R. Todt, X. F. Zhang, D. J. Miller, M. St. Louis-Weber, and V. P. Dravis, Appl. Phys. Lett. **69**, 3746 (1996).